

pubs.acs.org/IECR Article

A One-Step Facile Encapsulation of Zeolite Microcrystallites in Ordered Mesoporous Microspheres

Azeem Farinmade, Oluwole Ajumobi, Lei Yu, Yang Su, Jibao He, Julia A. Valla,* and Vijay John*



Cite This: Ind. Eng. Chem. Res. 2020, 59, 13923-13931



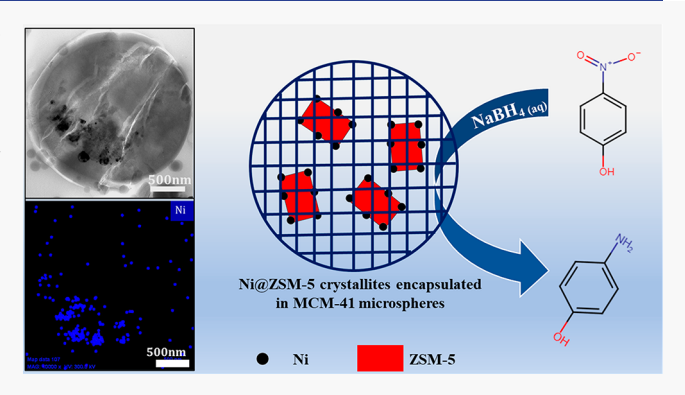
ACCESS

Metrics & More

Article Recommendations

3 Supporting Information

ABSTRACT: A facile aerosol-assisted technique was employed for the design of a new class of composite zeolite catalyst material with spherical morphology. This technique enables the one-step encapsulation of zeolite microcrystals into the matrix of spherical mesoporous silica particle supports such as MCM-41. By introducing presynthesized zeolite microcrystals into precursor solutions containing the templating surfactant and the silica precursor followed by aerosolization through nozzles larger than the microcrystals, it is possible to entrain the microcrystals in the aerosol droplet. Transport of the droplet through the heated zone of the furnace leads to hydrolysis and condensation of the silica precursor (tetraethyl orthosilicate, TEOS) in each droplet and the formation of spherical particles of MCM-41 containing embedded



zeolite microcrystals. This bottle-around-a-ship procedure to make zeolite-MCM-41 composites is extremely effective and can be easily scaled up. Detailed characterization of these composite particles reveals that up to 75 wt % of ZSM-5 zeolite can be embedded in MCM-41 microspheres with no loss of fidelity in particle morphology. To verify access of the reactants to the zeolite, we impregnated the ZSM-5 with nickel (Ni@ZSM-5) prior to encapsulation in MCM-41, and have shown the feasibility of the system to the model reaction of the liquid phase catalytic reduction of 4-nitrophenol to 4-aminophenol. While the reaction proceeds efficiently, there are diffusional restrictions to the transport of 4-nitrophenol resulting in a composite catalyst effectiveness factor of 0.4. The encapsulation of zeolite crystals within a micrometer-sized mesoporous MCM-41 shell provides structural stability to the zeolites and could reduce the pressure drop across a fixed bed tubular reactor due to the increased particle size of the composite. Potential applications of such composite particles include the ability of the MCM-41 to act as sacrificial adsorbents for coke and catalyst poisons, thus extending the life of the active material.

1. INTRODUCTION

Because of its well-defined micropores and high acidity, aluminosilicate ZSM-5 has been used as a catalyst in important petrochemical reactions such as methanol-to-hydrocarbons, 1-4 naphtha cracking⁵ and a host of other hydrocarbon conversions.⁶⁻⁸ Recent studies have shown that ZSM-5 is an effective catalyst for biomass conversion to fuels, as the acid catalytic sites favor deoxygenation reactions and the formation of light aromatic hydrocarbons. 9-11 However, access to interior catalytic sites of micrometer-sized ZSM-5 crystals is impeded by diffusional restrictions especially of larger reactants, and there is a need to use submicrometer ZSM-5 crystallites to enhance access to acidic sites. Such small particles are difficult to use in packed bed reactors because they give rise to high pressure drops. Thus, there is a need to integrate the small crystallites into a support material. Additionally, using supports that act as sacrificial sites for the adsorption of coke may lead to useful composite catalyst morphologies. 12,13

Several studies have reported the introduction of mesoporosity in ZSM-5 microcrystallite catalyst particles to facilitate enhanced access to catalytic sites.^{14–19} This can be done through multiple routes including the phase transformation of the ordered mesoporous structure of MCM-41 into ZSM-5 via recrystallization,¹⁶ partial desilication of large crystals of ZSM-5, and resilication in the presence of templating surfactants (cetyltrimethylammonium bromide, CTAB) to form hierarchical MCM-41/ZSM-5 composites²⁰ or the preparation of core—shell ZSM-5/MCM-41 composites where a shell of MCM-41 is formed by adsorbing the templating surfactant on the external surface of crystals of ZSM-5 followed by MCM-41 nucleation.^{21,22} While these methods lead to effective composites, they require multiple steps in composite synthesis and are difficult to scale up, and in the case of hierarchical

Received: April 24, 2020 Revised: July 6, 2020 Accepted: July 8, 2020 Published: July 8, 2020





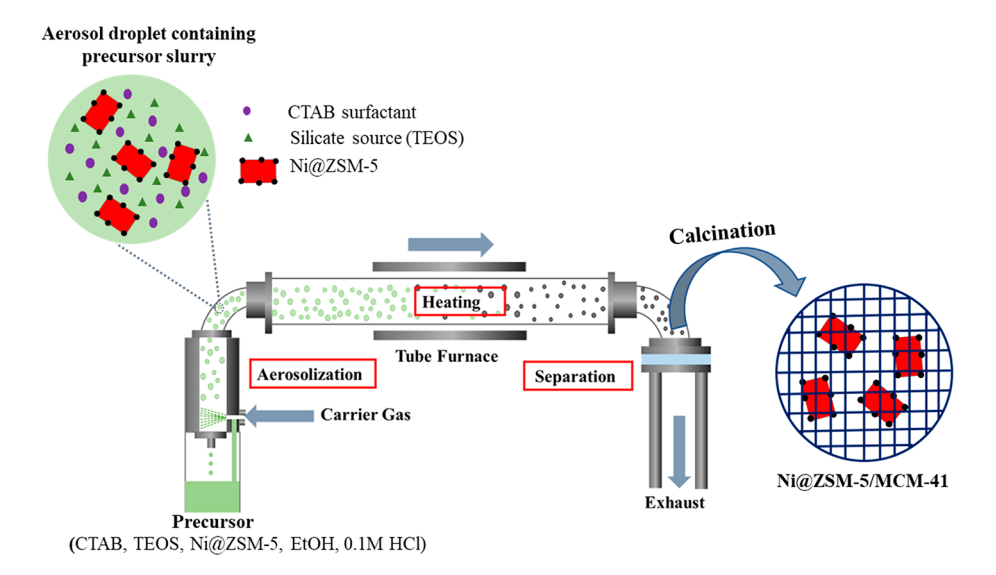


Figure 1. Schematic showing the setup for the aerosol-assisted synthesis procedure.

composites formed by desilication and resilication to MCM-41, there is a loss of acid sites. ^{23,24}

In this paper, we describe a one-step aerosol assisted method to achieve the rapid encapsulation of zeolite ZSM-5 microcrystals within the matrix of micrometer-sized MCM-41 spheres. The concept is a direct extension of the landmark work done by Lu and Brinker²⁵ where precursors to MCM-41 (tetraethyl orthosilicate, TEOS, and the cationic templating surfactant CTAB) are present in the feed solution which is aerosolized, and the aerosol droplets are passed through a heated zone to evaporate the solvent and form MCM-41 through hydrolysis and templated condensation. This facile aerosol-assisted synthesis technique has since been developed and adapted for the synthesis of spherical heterogeneous composite catalysts. 26,27 A comprehensive review by Debecker et al.26 describes recent advances in developing catalytic materials through spray drying. Spherical aggregates of hierarchical zeolites with unique compositions and applications have been synthesized via the aerosol-assisted technique.^{27–30} These aggregated zeolitic microspheres often have binders or fillers such as polymers, nanoclays, silica, and alumina incorporated into their matrix to impact mechanical stability or reaction selectivity. 28,30,31 However, pore-structure hierarchical catalysts in which active microporous zeolite are completely encapsulated in the matrix of inert spherical mesoporous silica supports via aerosol synthesis has not been reported in the literature and is the subject of our work. To integrate zeolites into the matrix of MCM-41, it was our objective to simply add presynthesized ZSM-5 microcrystals to the precursor solution to form a slurry that is then aerosolized. It was our hypothesis that the ZSM-5 microcrystals would be entrained in the droplets and the synthesis of MCM-41 in the droplets would lead to spherical composites of ZSM-5 distributed in a matrix of MCM-41. Figure 1 illustrates the concept in which calcination of the product collected over a filter leads to burnoff of the templating agent and the formation of a solid particle of MCM-41 with encapsulated

This paper describes the feasibility of the process and the detailed characterization of the materials. Access to ZSM-5 is done through a model reaction through which Ni clusters are immobilized on the ZSM-5 microcrystals to catalyze the model

reaction of the reduction of 4-nitrophenol to 4-aminophenol as shown in Scheme 1.

Scheme 1. Conversion Sequence for the Catalytic Reduction of 4-Nitrophenol to 4-Aminophenol

2. EXPERIMENTAL SECTION

2.1. Materials. Hexadecyltrimethylammonium bromide (CTAB, 95%), nickel(II) nitrate hexahydrate (Ni(NO₃)₂· 6H₂O), tetraethyl orthosilicate (TEOS, 98%), hydrochloric acid (HCl, 37%), sodium borohydride (NaBH₄), and 4-nitrophenol (10 mM) were purchased from Sigma-Aldrich and were used without any modifications. ZSM-5 was purchased from Zeolyst International (Product No. CBV8014) and was first calcined in air at 550 °C for 6 h to obtain zeolite in H⁺ form before use. Deionized (DI) water with a resistance of 18.2 M Ω was obtained from an Elga water purification system (Medica DV25).

2.2. Synthesis of Ni@ZSM-5 and Ni Nanoparticles. Calcined ZSM-5 was used as the parent material for the preparation of Ni@ZSM-5 catalyst. ZSM-5 was impregnated with 10 wt % of Ni using an incipient wetness impregnation method. Nickel(II) nitrate hexahydrate (Ni(NO₃)₂·6H₂O) solution was prepared by dissolving Ni(NO₃)₂·6H₂O crystals in the amount of water needed to saturate ZSM-5. The solution was then added dropwise to ZSM-5 with stirring until the precursor solution was used up. The prepared mixture was then dried at 80 °C for 12 h after which the dried material was crushed and calcined at 550 °C in air for 2 h. The final product was obtained by reducing the material in H₂ at 550 °C for 4 h. Nickel-impregnated ZSM-5 is thus abbreviated as Ni@ZSM-5.

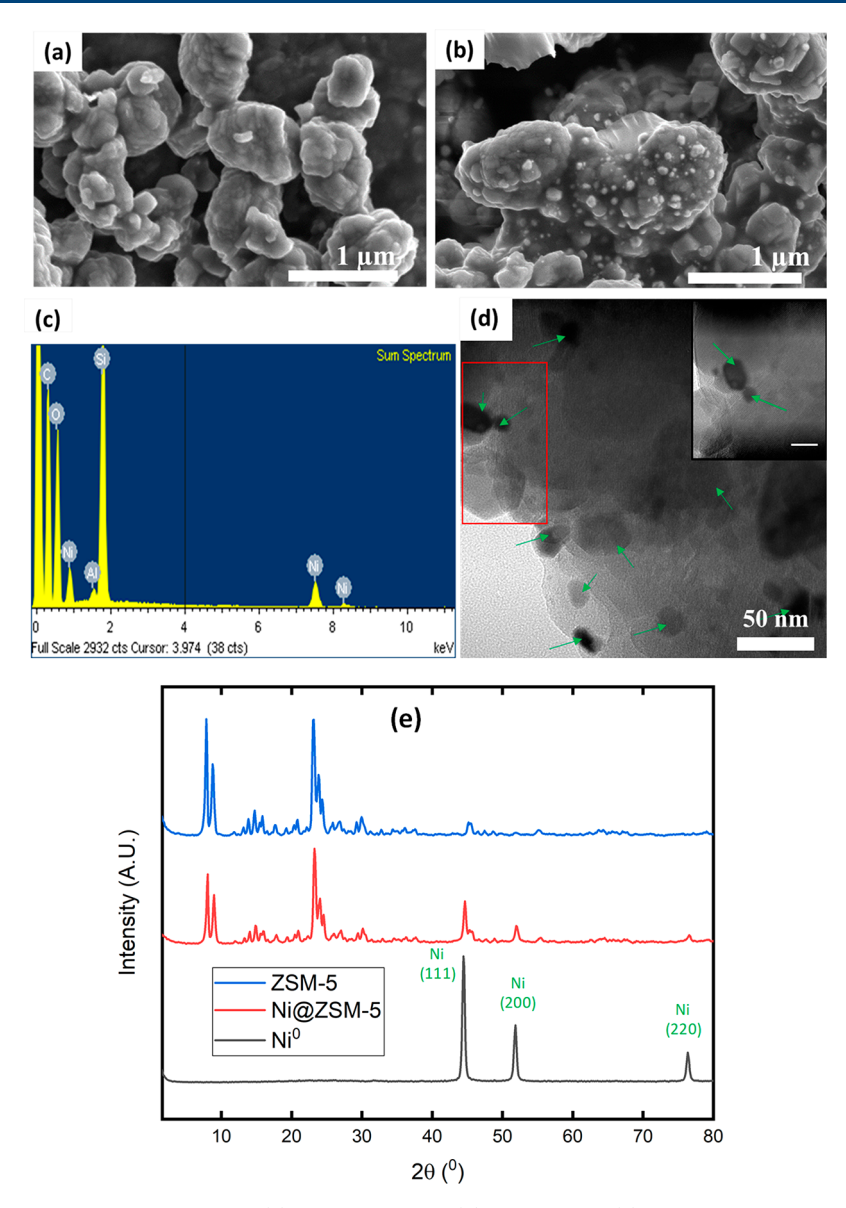


Figure 2. SEM images showing surface morphology of (a) bare ZSM-5 and (b) Ni@ZSM-5; (c) SEM-EDS confirming the presence of Ni in Ni@ZSM-5; (d) TEM images of Ni@ZSM-5 showing size distribution of Ni on ZSM-5. Inset is a high magnification image that clearly shows the contrast between the Ni nanoparticles and the ZSM-5 support (inset scale bar = 20 nm). (e) XRD analysis of Ni@ZSM-5 showing the additional Ni peaks corresponding to the 111, 200, and 220 planes of Ni in addition to the characteristic ZSM-5 diffraction peaks.

Unsupported Ni nanoparticle was synthesized using an already established technique with some modifications. Briefly, 0.2 g of nickel(II) nitrate hexahydrate (Ni(NO₃)₂·6H₂O) was dissolved in 50 mL of ethanol under magnetic stirring in a flask. An excess of 0.05 M NaBH_{4(aq)} was titrated dropwise against the salt solution until the color of the solution changed completely from green to black indicating the complete reduction of Ni²⁺ to Ni⁰. The suspension was centrifuged to recover the particles and was washed several times with ethanol before drying under vacuum at 80 °C.

2.3. Encapsulation of ZSM-5 and Ni@ZSM-5 in MCM-41. The one-step encapsulation of zeolites was achieved by an aerosol-assisted technique previously reported for the synthesis of hollow and mesoporous silica particles. ^{25,33,34} To prepare the aerosol precursor solution, 1.5 g of cetyltrimethylammonium bromide (CTAB) was weighed into a vial containing 15 mL of ethanol and allowed to dissolve under magnetic stirring. Ni@ZSM-5 (0.29 g, for 25 wt % Ni@ZSM-5 in composite)

was added to the CTAB solution and sonicated in a bath sonicator (Cole-Parmer 8890) for 1 min to disperse the zeolites evenly in the solution. The suspension of zeolites in surfactant (CTAB) solution was stirred continuously using a magnetic stirrer, then 6.75 mL of tetraethyl orthosilicate (TEOS, 98%) was added dropwise. Two milliliters of 0.1 M HCl was then added to the suspension, and the mixture was allowed to stir for 30 min. The preparation of this precursor solution was carried out at room temperature. The precursor solution was then transferred into an inexpensive nebulizer (Micro Mist, Teleflex Inc., 1 mm jet hole diameter) and carried into the heating chamber using N2 gas flowing at approximately 2.5 L/min as the carrier gas. The heating chamber is basically a quartz tube with internal diameter of 5 cm and length of 120 cm which is inserted into a furnace that is 76 cm in length and operating isothermally at 400 $^{\circ}\text{C}$ as illustrated by Figure 1. The dimensions of the furnace (76 cm) and flow rate of the carrier gas (2.5 L/min) allow a short

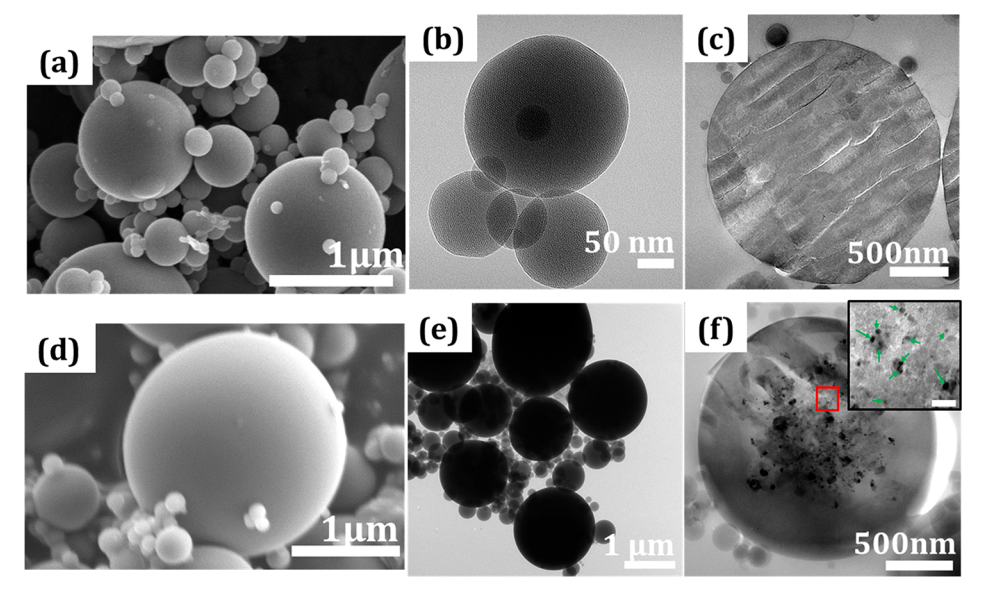


Figure 3. Contrasting the morphologies of bare MCM-41 particles to those of the synthesized Ni@ZSM-5 composite: (a-c) SEM, TEM, and cut-section TEM images of bare MCM-41; (d-f) SEM, TEM, and cut-section TEM of 25-Ni@ZSM-5/MCM-41. Cut-section TEM images of 25-Ni@ZSM-5/MCM-41 provides clear visualization of Ni supported on encapsulated Ni@ZSM-5 within the MCM-41 microsphere matrix (inset scale bar = 50 nm).

residence time of approximately 36 s in the furnace heating zone. At the other end of the tube, the dried particles are collected by a filter paper (Merck Millipore Ltd., pore size = $0.22 \mu m$) which was kept constant at 80 °C by heating coils to avoid moisture condensation. The particles were then collected and calcined in air at 550 °C for 6 h at a heating rate of 5 °C/ min to burn off the surfactant template. Composites of 50 and 75 wt % were also synthesized by varying the mass of Ni@ ZSM-5 to the volume of TEOS in the precursor. Composites containing Ni@ZSM-5 were treated with H₂ at 550 °C for 4 h to obtain Ni in reduced form. As a control, bare MCM-41 particles were also synthesized using the same methodology and quantities of reagents except for the addition of Ni@ZSM-5. The composite materials are hereby labeled X-ZSM-5/ MCM-41 for ZSM-5 encapsulated in MCM-41 and X-Ni@ ZSM-5/MCM-41 for nickel-impregnated ZSM-5 encapsulated in MCM-41 where the prefix X stands for the theoretical weight percent of ZSM-5 or Ni@ZSM-5 to MCM-41 in the composite.

2.4. Materials Characterization. The morphology of the synthesized particles was visualized using scanning electron microscopy (SEM, Hitachi S-4800 field emission scanning electron microscope operated at 3 kV) and transmission electron microscopy (TEM, FEI Tecnai G2 F30 twin transmission electron microscope operated at 300 kV). Transmission electron microscope operat

2.5. Catalytic Activity of Ni@ZSM-5/MCM-41 Composite. To ascertain that reactants can access the encapsulated zeolites through the porous MCM-41 shell, we tested the catalytic activity of Ni@ZSM-5 encapsulated in MCM-41 using the catalytic reduction of 4-nitrophenol (4-NP) to 4-aminophenol (4-AP) as a model reaction. The reduction of 4-

nitrophenol to 4-nitrophenolate intermediate product occurs in the presence of excess NaBH4 which acts as a reducing agent while an active metal catalyst is required to lower the activation energy to favor the formation of the 4-aminophenol final product.^{37,38} First, to test the efficacy of the catalysts to 4nitrophenol reduction, we conducted a batch reaction wherein 5 mg of catalysts (Ni@ZSM-5 and 50-Ni@ZSM-5/MCM-41) were introduced into a vial containing 1.5 mL of 0.05 mM 4nitrophenol and 1.5 mL of 0.02 M NaBH₄ and allowed to sit for 2 h. The UV absorbance before the introduction of catalysts and 2 h after introducing the catalysts was measured using Shimadzu UV-1700 PharmaSpec UV-vis spectrophotometer to determine the conversion of 4-nitrophenol to 4aminophenol. To study the reaction kinetics for the 4nitrophenol reduction, 15 mL of 0.1 M NaBH₄ was added to 5 mL of 0.1 mM 4-nitrophenol in a glass vial and stirred magnetically. The desired mass of Ni@ZSM-5 or Ni@ZSM-5/ MCM-41 was then added to initiate the reaction. The reaction was monitored via UV-vis spectroscopy by sampling 1.5 mL at different time intervals. The sampled reactants were replaced in the reaction vial after each analysis to conserve the catalyst. The rate of reaction was obtained by measuring the UV absorbance of the 4-nitrophenolate peak at 400 nm with time. The reaction was completed once the 4-nitrophenolate peak at 400 nm completely disappears with simultaneous appearance of the 4-aminophenol peak at 300 nm.

3.0. RESULTS AND DISCUSSION

3.1. Synthesis and Materials Characterization. The synthesis of Ni on ZSM-5 catalyst (Ni@ZSM-5) was achieved via wet impregnation of nickel salt and subsequent reduction in the presence of H_2 gas.^{39,40} Figure 2a shows an SEM image of the pristine ZSM-5 prior to impregnation of Ni. We observe the agglomeration of cubic particles characteristic of ZSM- $5^{14,15}$ with individual particle sizes of 100-300 nm. Upon impregnation of 10 wt % Ni on ZSM-5, we observe some surface roughening indicative of nanosized Ni particles tethered across the surface of the ZSM-5 as shown in the

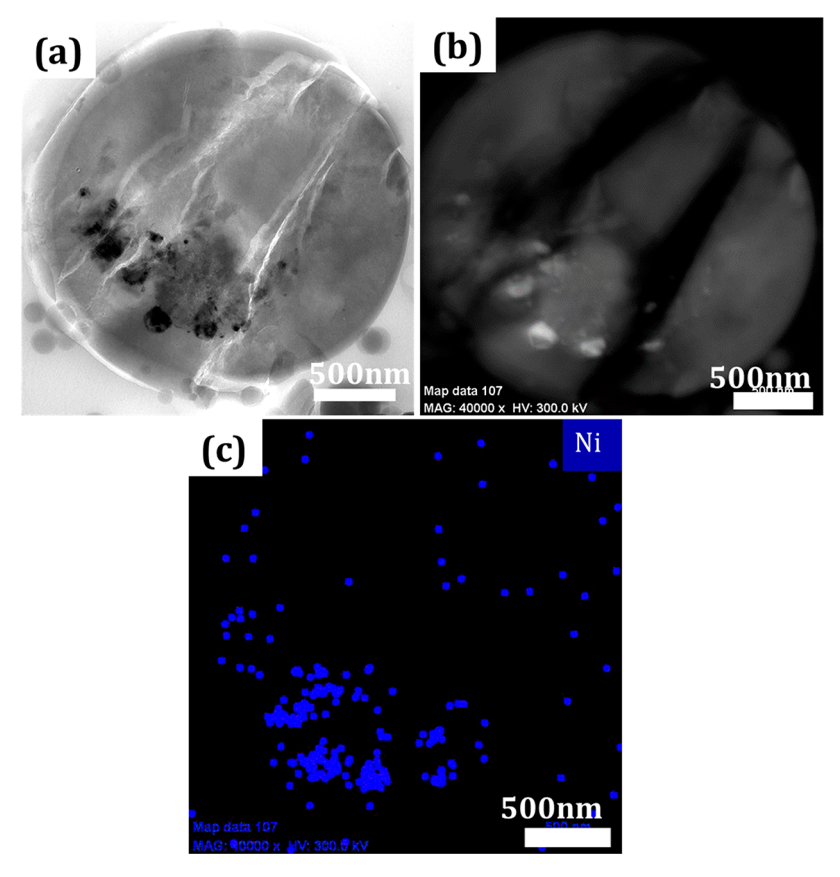


Figure 4. Electron microscopy images of cut-sections of a 25-Ni@ZSM-5/MCM-41 composite particle: (a) TEM, (b) STEM, and (c) STEM-EDS mapping shows the location of Ni nanoparticles supported on ZSM-5 encapsulates within the spherical MCM-41 shell. Graph showing the complete elemental composition of the particle is provided in the Supporting Information section S1.

SEM image of Figure 2b. The presence of Ni on the ZSM-5 support was further confirmed by carrying out energy dispersive X-ray spectroscopy (SEM-EDS) to obtain elemental analysis across a 50 nm section of the Ni@ZSM-5 surface as shown in Figure 2c. Figure 2d provides a high resolution TEM image of the Ni@ZSM-5 to clearly visualize the electron dense Ni nanoparticles dispersed on the ZSM-5 support with nanoparticle size ranging from 5 to 50 nm. Figure 2e shows the XRD structural analysis for the ZSM-5 with characteristic diffraction peaks. 41,42 Upon impregnating the ZSM-5 with Ni, we observe the additional peaks corresponding to the (111), (200), and (220) planes of Ni. 43

The encapsulation of ZSM-5 crystals within the matrix of the mesoporous MCM-41 microspheres was achieved by a onestep aerosol-assisted technique as illustrated in Figure 1.^{25,33} The precursor for aerosolization was a stirred slurry of ZSM-5 (or Ni@ZSM-5) particles in a solution containing the precursors for MCM-41 (CTAB, TEOS in ethanol with 0.1 M HCl) with the composition already described in the Experimental Section. The orifice size of 1 mm is significantly larger than the particle size allowing the particles to be carried by N₂ gas through the orifice and be encapsulated in the aerosol droplets. Such "chemistry in a droplet" proceeds as each aerosol droplet carried into the furnace heating zone acts like a microreactor for the rapid hydrolysis and condensation of TEOS to silica.²⁵ In the confined environment of the droplet, hydrolysis and condensation of TEOS to silica starts at the exterior of the droplet and rapidly moves inward, and ceramic particulates in the droplet (ZSM-5 or Ni@ZSM-5 particles) become entrapped within the matrix of the silica that

is formed. The inclusion of CTAB in the precursor droplet results in templating to MCM-41, and the zeolite microcrystals are captured in the ordered mesoporous matrix. Subsequent calcination leads to removal of the CTAB and the final morphology of ZSM-5 or Ni@ZSM-5 embedded in the mesoporous matrix. Figure 3a shows a SEM image of MCM-41 synthesized by the aerosol technique. The aerosol process inherently leads to a large degree of polydispersity but we note that with the inexpensive nozzles used we are able to obtain high particle throughputs (>2 g in 30 min) and each particle regardless of its size has the ordered mesoporous characteristics of MCM-41 as indicated by the TEM images of Figure 3b. 44,45 Figure 3 panels d and e are SEM and TEM images of composite particles of Ni@ZSM-5 encapsulated in MCM-41 (25-Ni@ZSM-5/MCM-41), respectively. Both images show that we obtain the spherical morphologies as in the bare MCM-41 (Figure 3a,b) and that there is no evidence of zeolite microparticles external to the MCM-41 particles or embedded on the surface of the MCM-41 particles. Clear evidence of zeolite encapsulation is provided by the cut section TEM images of a 25-Ni@ZSM-5/MCM-41particle which shows Ni containing zeolites embedded in the MCM-41 matrix. The inset to Figure 3f is a high resolution TEM of the cut section showing further details of the distribution of the Ni@ZSM-5 crystals within the MCM-41 matrix.

Scanning transmission electron microscopy (STEM) and STEM-EDS elemental analysis were used to obtain the elemental composition on the cut-section image of a 25-Ni@ZSM-5/MCM-41 particle and confirmed that the dark spots shown on the cut section images are truly Ni particles (Figure

4). Figure 4a is the cut section TEM image of a 25-Ni@ZSM-5/MCM-41 particle and Figure 4b is the corresponding STEM image where the Z-contrast shows the reflection of the Ni particles. STEM-EDS elemental mapping of Ni in the particle cut section (Figure 4c) verifies the presence of Ni and, thus indirectly, the location of the ZSM-5 microcrystals. We note that the nonuniformity of zeolite distribution in Figure 4 may be the result of the plane across which the cut section was obtained rather than an intrinsic nonuniformity of zeolite embedding.

BET surface areas and X-ray diffraction patterns of all samples used are shown in Figure 5, and the results are

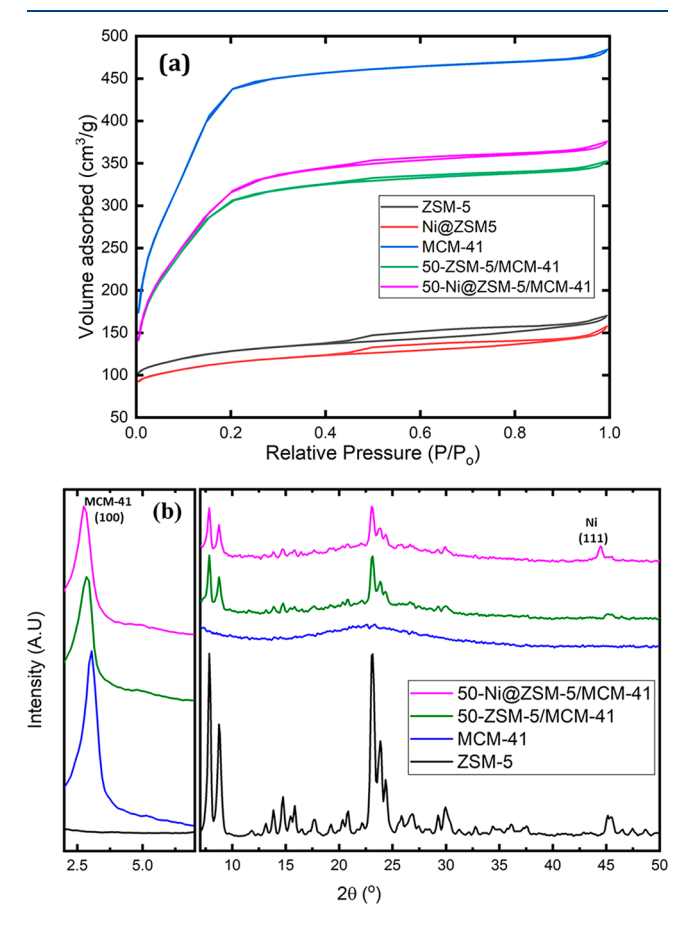


Figure 5. (a) BET isotherm plot for ZSM-5, Ni@ZSM-5, MCM-41, 50-ZSM-5/MCM-41, and 50-Ni@ZSM-5/MCM-41; (b) XRD patterns for ZSM-5, MCM-41, 50-ZSM-5/MCM-41, and 50-Ni@ ZSM-5/MCM-41.

tabulated in Table 1. As expected, mesoporous MCM-41 has a high surface area 1380 m²/g while the microporous ZSM-5 has a surface area of 398 m 2 /g. The composites (50-ZSM-5/ MCM-41 and 50-Ni@ZSM-5/MCM-41 samples) show surface areas that are close to the weighted average of the

Table 1. BET Surface Area Analysis

samples	BET surface area $\left(m^2/g\right)$
ZSM-5	398
Ni@ZSM5	359
MCM-41	1380
50-ZSM-5/MCM-41	965
50-Ni@ZSM-5/MCM-41	1030

individual surface areas regardless of the presence of Ni. X-ray diffraction (XRD) structural analysis on the synthesized composite materials and the diffraction patterns are shown in Figure 5b. The control of bare MCM-41 material shows the characteristic (100) diffraction peak at $2\theta = 2.9^{\circ}$ which corresponds to a d-spacing of approximately 3 nm. 46 Figure S4 in the Supporting Information shows a high resolution smallangle X-ray scattering pattern of the MCM-41 where we can clearly visualize the higher order (110) and (200) peaks in addition to the primary (100) peak. Analysis of the SAXS peaks shown in Table S2 confirms the d-spacing (2.9 nm) of the primary peak and the q-ratios of the higher order peaks confirm the hexagonal structure that is characteristic of MCM-41. For the composite 50-ZSM-5/MCM-41 material, additional diffraction peaks associated with the (101), (111), (051), (313), and (323) planes of ZSM-5, respectively, are observed. The 50-Ni@ZSM-5/MCM-41 material further shows a peak at $2\theta = 44.7^{\circ}$ associated with the (111) plane of Ni. Together with the imaging data that indicate encapsulation of Ni@ZSM-5 in the MCM-41 matrix, it is evident that the synthesis technique maintains structural integrity of all components. We have been able to integrate up to 75 wt % Ni@ZSM-5 into MCM-41 (Supporting Information S2) but observe some segregation of structure in the composite particles at these high loadings of Ni@ZSM-5 and a possible loss of ordering of the MCM-41.

3.2. Access to Catalytic Sites. Particle characterizations thus indicate that the Ni@ZSM-5 is distributed in the matrix of MCM-41 and that this may lead to more efficient packing of the zeolite microcrystals in reactors. However, it is necessary to show that reactants can access the encapsulated zeolite microcrystals. Thus, verification of the catalytic activity of Ni@ZSM-5 in the composite is equivalent to verifying accessibility to zeolite active zeolite/metal species within the inert mesoporous MCM-41 matrix. We have therefore used the liquid-phase catalytic reduction of 4-nitrophenol (4-NP) to 4aminophenol (4-AP) in the presence of excess sodium borohydride (NaBH₄) as a model reaction to investigate the catalytic activity of the Ni@ZSM-5/MCM-41 composite catalyst. Figure 6a illustrates the overall reaction in which the 4-nitrophenolate absorbance (400 nm) observed at t = 0 is entirely replaced by the 4-aminophenol absorbance at 300 nm after completion of the reaction. Both Ni@ZSM-5 and 50-Ni@ ZSM-5/MCM-41 show full conversions within 2 h of reaction. We note that the control of bare MCM-41 is inactive for the reaction but does show the adsorption of approximately 25% of the nitrophenol (Supporting Information S3).

Figure 6d shows the kinetics of the reaction, with the regressed lines showing fits from pseudo-first-order kinetics. When normalized based on the amount of Ni in the sample, the observed pseudo-first-order rate constants ($k_{\rm obs}$) are 8.3 s^{-1}/g for Ni@ZSM-5 and 3.19 s^{-1}/g for Ni@ZSM-5/MCM-41. Thus, there is an observed 50% reduction in observed rate when the Ni@ZSM-5 crystallites are embedded in MCM-41. This is clearly the consequence of diffusional restrictions in the mesoporous matrix as shown by the data in Figures 6b-d. If we assume that the presence of Ni on the external surface of Ni@ZSM-5 indicates a system with no diffusional restrictions with the catalyst effectiveness factor of unity, then the effectiveness factor of particles of 50-Ni@ZSM-5/MCM-41 is the ratio of the observed rate constants or 0.4. This is entirely reasonable for the 0.7 nm nitrophenol species (end to end length was obtained from Avogadro: an open-source molecular

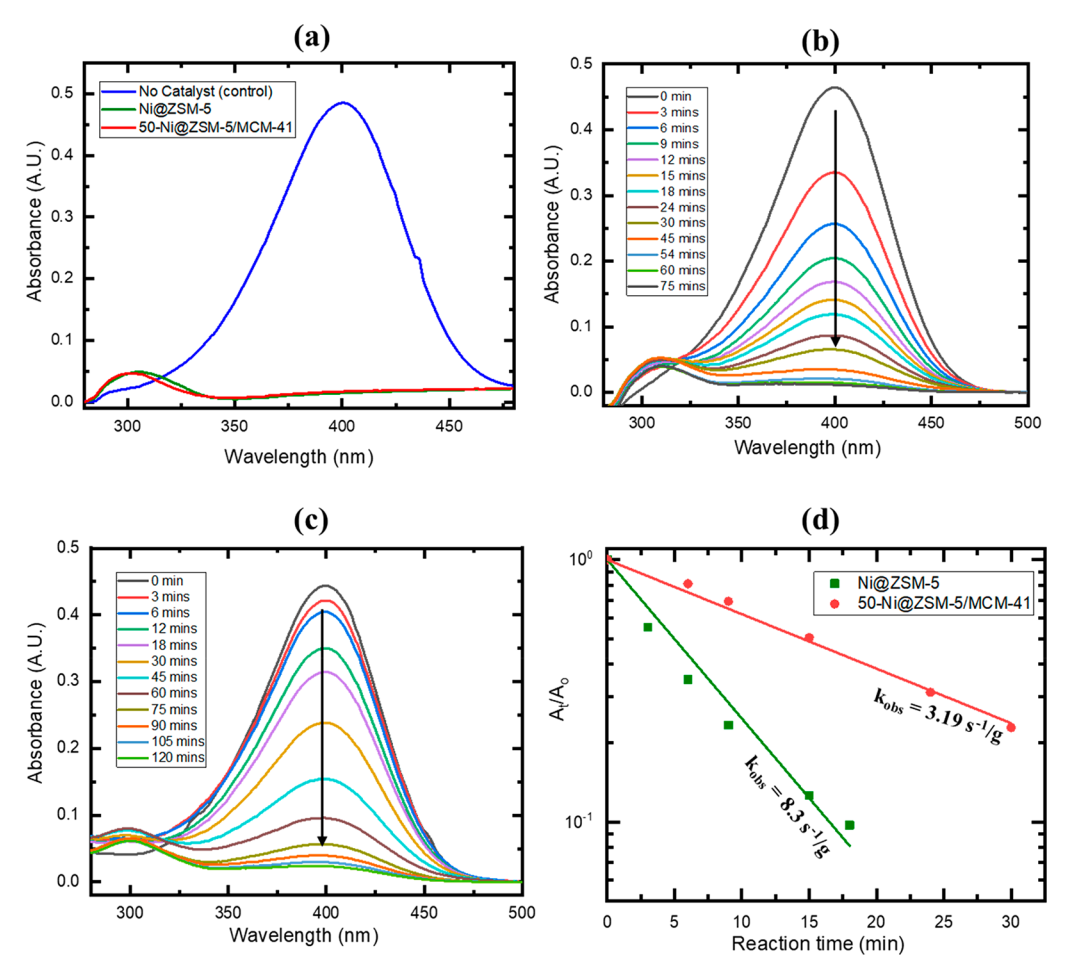


Figure 6. Reduction of 4-nitrophenol to 4-aminophenol: (a) UV—vis absorption spectra shows the complete conversion of 4-nitrophenol to 4-aminophenol after 2 h reaction time by Ni@ZSM-5 and 50-Ni@ZSM-5/MCM-41 catalysts; (b) UV—vis spectra for the reduction of 4-NP by Ni@ZSM-5; (c) UV—vis spectra for the reduction of 4-NP by 50-Ni@ZSM-5/MCM-41; (d) kinetics of 4-nitrophenol reduction by Ni@ZSM-5 and 50-Ni@ZSM-5/MCM-41.

builder and visualization tool version 1.2 developed by the Avogadro Project, USA) diffusing through the 3 nm channels of MCM-41. The fact that MCM-41 adsorbs nitrophenol may further restrict pore dimensions to diffusion, and the observed reaction in these composite pellets essentially couples adsorption, diffusion, and intrinsic reaction. However, the relatively low level of adsorption of 4-nitrophenol onto MCM-41 (Figure S3) implies that most of the decrease in the reaction rate is perhaps due to diffusional restrictions. Irreversible Ni site suppression may also contribute to the reduced reaction rates in the Ni@ZSM-5/MCM-41 composite, whereby the external silica matrix overlays some of the Ni crystallites supported on the ZSM-5 and prevents reactants from accessing these active sites. However, we do not expect this to be the case with the interior acid sites of the zeolites, and this will not hinder the applicability of these composites to hydrodeoxygenation-type reactions in which the acid sites of ZSM-5 play an active role. Nevertheless, it is clear that a high rate of reaction is entirely feasible in these systems and that ZSM-5 is accessible to reactants when it is immobilized in the MCM-41 microspheres through the aerosol-assisted process.

4.0. CONCLUSIONS

This study presents a new class of composite zeolite catalyst materials wherein zeolite microcrystals are embedded and distributed in a matrix of a spherical particle of the ordered mesoporous MCM-41. The encapsulation of presynthesized zeolite microcrystals in the matrix of MCM-41 is done in a one-step aerosol technique by which MCM-41 is synthesized in the confined environment of an aerosol droplet which contains the zeolite microcrystals. The technique involves small residence times for synthesis and can be adapted to a continuous process. Up to 75 wt % loading of the MCM-41 matrix with the zeolite microcrystals can be obtained without a significant distortion in overall particle morphology. By placing Ni clusters on the ZSM-5 external surface, it was verified that the zeolite becomes accessible to reactants through the model reaction of nitrophenol reduction to aminophenol.

We have thus developed a facile method of distributing zeolite microcrystals in a mesoporous material that may enable a packed bed reactor design with minimal pressure drops across the bed and with control of reaction heat effects by the loading of material in the MCM-41. This is a model of the egg—yolk type catalyst morphology in which the active material is within an inactive matrix and for which the matrix can serve as an adsorbent for either catalytic poisons (sulfur containing compounds, remnant feed organometallics, etc.) or to enhance concentrations of reactant so that local reactant concentrations in the vicinity of the acid catalytic sites are increased. While there could be transport limitations through the pores of MCM-41 especially in the case of large reactants

and products, the accessibility to zeolite catalytic sites within a structurally stable matrix could be a trade-off without the need to create mesoporosity in large zeolite crystals by partially etching away the zeolite. ⁴⁷ When fabricated into catalyst pellets for fixed bed reactors, we envision three hierarchical pore structures: the microporosity of the zeolite, the mesoporosity of the MCM-14, and the pellet macroporosity imposed by binders. Thus, there is the potential for tuning reaction and diffusion.

Continued work seeks to apply such composite catalysts to industrially relevant reactions. Of particular interest, our continued work seeks to address the use of these composite catalysts in the upgrade of biofuels with the use of ZSM-5 for deoxygenation and hydrocarbons production, for which the MCM-41 may serve as a sacrificial layer for coke formation, thus reducing the rate of deactivation of the zeolite.⁴⁸ It is relatively easy to integrate other metals into the matrix by simply including these in the precursor feed to the aerosol. For example, a Pt precursor could be integrated into the solution resulting in Pt clusters in the mesoporous silica matrix. The proximity to the zeolite would result in true bifunctional catalysis for hydrogenation/dehydrogenation on Pt and acid catalyzed isomerization on the zeolite. This may lead to new concepts in hydroisomerization and catalytic reforming, and such aspects are the focus of our continuing studies.

ASSOCIATED CONTENT

Supporting Information

The Supporting Information is available free of charge at https://pubs.acs.org/doi/10.1021/acs.iecr.0c02054.

STEM-EDS elemental analysis of the cut-section of a Ni@ZSM-5/MCM-41 particle; effect of Ni@ZSM-5 loading on the extent of encapsulation; adsorption of 4-nitrophenol by MCM-41; small angle X-ray scattering (SAXS); powder diffraction analysis (PDF)

■ AUTHOR INFORMATION

Corresponding Authors

Vijay John — Department of Chemical & Biomolecular Engineering, Tulane University, New Orleans, Louisiana 70118, United States; ⊚ orcid.org/0000-0001-5426-7585; Email: vj@tulane.edu

Julia A. Valla – Department of Chemical & Biomolecular Engineering, University of Connecticut, Storrs, Connecticut 06269, United States; Email: ioulia.valla@uconn.edu

Authors

Azeem Farinmade — Department of Chemical & Biomolecular Engineering, Tulane University, New Orleans, Louisiana 70118, United States; orcid.org/0000-0003-1343-9496

Oluwole Ajumobi — Department of Chemical & Biomolecular Engineering, Tulane University, New Orleans, Louisiana 70118, United States; orcid.org/0000-0003-4356-7923

Lei Yu – Department of Chemical & Biomolecular Engineering, University of Connecticut, Storrs, Connecticut 06269, United States

Yang Su — Department of Chemical & Biomolecular Engineering, Tulane University, New Orleans, Louisiana 70118, United States

Jibao He – Coordinated Instrumentation Facility, Tulane University, New Orleans, Louisiana 70118, United States

Complete contact information is available at:

https://pubs.acs.org/10.1021/acs.iecr.0c02054

Notes

The authors declare no competing financial interest.

ACKNOWLEDGMENTS

We gratefully acknowledge funding from the National Science Foundation (NSF Grant No. 1826146) and the Louisiana Board of Regents. Dr. Miriam Siebenbuerger from the Center for Advanced Microstructures and Devices (CAMD) at Louisiana State University is also acknowledged for assistance in small-angle X-ray scattering measurements.

REFERENCES

- (1) Ono, Y.; Mori, T. Mechanism of Methanol Conversion into Hydrocarbons over ZSM-5 Zeolite. *J. Chem. Soc., Faraday Trans.* 1 1981, 77 (9), 2209–2221.
- (2) Haw, J. F.; Song, W.; Marcus, D. M.; Nicholas, J. B. The Mechanism of Methanol to Hydrocarbon Catalysis. *Acc. Chem. Res.* **2003**, *36* (5), 317–26.
- (3) Ilias, S.; Bhan, A. Mechanism of the Catalytic Conversion of Methanol to Hydrocarbons. *ACS Catal.* **2013**, 3 (1), 18–31.
- (4) Wang, J.; Gao, X.; Chen, G.; Ding, C. Forming Pure Shaped ZSM-5 Zeolite Bodies by a Steam-Assisted Method and Their Application in Methanol to Aromatic Reactions. *RSC Adv.* **2019**, 9 (49), 28451–28459.
- (5) Yoshimura, Y.; Kijima, N.; Hayakawa, T.; Murata, K.; Suzuki, K.; Mizukami, F.; Matano, K.; Konishi, T.; Oikawa, T.; Saito, M.; Shiojima, T.; Shiozawa, K.; Wakui, K.; Sawada, G.; Sato, K.; Matsuo, S.; Yamaoka, N. Catalytic Cracking of Naphtha to Light Olefins. *Catal. Surv. Jpn.* **2001**, *4* (2), 157–167.
- (6) Ding, W.; Li, S.; D Meitzner, G.; Iglesia, E. Methane Conversion to Aromatics on Mo/H-ZSM5: Structure of Molybdenum Species in Working Catalysts. *J. Phys. Chem. B* **2001**, *105* (2), 506–513.
- (7) Isoda, T.; Nakahara, T.; Kusakabe, K.; Morooka, S. Catalytic Cracking of Polyethylene-Liquefied Oil over Amorphous Aluminosilicate Catalysts. *Energy Fuels* **1998**, *12* (6), 1161–1167.
- (8) Carlson, T. R.; Cheng, Y. T.; Jae, J.; Huber, G. W. Production of Green Aromatics and Olefins by Catalytic Fast Pyrolysis of Wood Sawdust. *Energy Environ. Sci.* **2011**, *4* (1), 145–161.
- (9) Gamliel, D. P.; Du, S.; Bollas, G. M.; Valla, J. A. Investigation of in Situ and Ex Situ Catalytic Pyrolysis of Miscanthus X Giganteus Using a Pygc-Ms Microsystem and Comparison with a Bench-Scale Spouted-Bed Reactor. *Bioresour. Technol.* **2015**, *191*, 187–96.
- (10) Jae, J.; Tompsett, G. A.; Foster, A. J.; Hammond, K. D.; Auerbach, S. M.; Lobo, R. F.; Huber, G. W. Investigation into the Shape Selectivity of Zeolite Catalysts for Biomass Conversion. *J. Catal.* **2011**, 279 (2), 257–268.
- (11) Gamliel, D. P.; Bollas, G. M.; Valla, J. A. Two-Stage Catalytic Fast Hydropyrolysis of Biomass for the Production of Drop-in Biofuel. *Fuel* **2018**, *216*, 160–170.
- (12) Mitchell, S.; Michels, N. L.; Perez-Ramirez, J. From Powder to Technical Body: The Undervalued Science of Catalyst Scale Up. Chem. Soc. Rev. 2013, 42 (14), 6094–112.
- (13) Shoinkhorova, T.; Dikhtiarenko, A.; Ramirez, A.; Dutta Chowdhury, A.; Caglayan, M.; Vittenet, J.; Bendjeriou-Sedjerari, A.; Ali, O. S.; Morales-Osorio, I.; Xu, W.; Gascon, J. Shaping of ZSM-5-Based Catalysts Via Spray Drying: Effect on Methanol-to-Olefins Performance. ACS Appl. Mater. Interfaces 2019, 11 (47), 44133—44143
- (14) Xia, Y.; Mokaya, R. On the Synthesis and Characterization of ZSM-5/MCM-48 Aluminosilicate Composite Materials. *J. Mater. Chem.* **2004**, 14 (5), 863–870.
- (15) Li, R.; Chong, S.; Altaf, N.; Gao, Y.; Louis, B.; Wang, Q. Synthesis of ZSM-5/Siliceous Zeolite Composites for Improvement of Hydrophobic Adsorption of Volatile Organic Compounds. *Front. Chem.* **2019**, *7*, 505.

- (16) Huang, L.; Guo, W.; Deng, P.; Xue, Z.; Li, Q. Investigation of Synthesizing MCM-41/ZSM-5 Composites. J. Phys. Chem. B 2000, 104 (13), 2817–2823.
- (17) Ooi, Y.-S.; Zakaria, R.; Mohamed, A. R.; Bhatia, S. Catalytic Cracking of Used Palm Oil and Palm Oil Fatty Acids Mixture for the Production of Liquid Fuel: Kinetic Modeling. *Energy Fuels* **2004**, *18* (5), 1555–1561.
- (18) Gou, J. S.; Wang, Z. P.; Li, C.; Qi, X. D.; Vattipalli, V.; Cheng, Y. T.; Huber, G.; Conner, W. C.; Dauenhauer, P. J.; Mountziaris, T. J.; Fan, W. The Effects of ZSM-5 Mesoporosity and Morphology on the Catalytic Fast Pyrolysis of Furan. *Green Chem.* **2017**, *19* (15), 3549–3557.
- (19) Na, J. D.; Liu, G. Z.; Zhou, T. Y.; Ding, G. C.; Hu, S. L.; Wang, L. Synthesis and Catalytic Performance of ZSM-5/MCM-41 Zeolites with Varying Mesopore Size by Surfactant-Directed Recrystallization. *Catal. Lett.* **2013**, *143* (3), 267–275.
- (20) Gamliel, D. P.; Cho, H. J.; Fan, W.; Valla, J. A. On the Effectiveness of Tailored Mesoporous Mfi Zeolites for Biomass Catalytic Fast Pyrolysis. *Appl. Catal., A* **2016**, *522*, 109–119.
- (21) Li, Z.; Zhong, Z.; Zhang, B.; Gu, J.; Shi, K. Catalytic Fast Pyrolysis of Bamboo over Micro-Mesoporous Composite Molecular Sieves. *Energy Technology* **2018**, *6*, 728–736.
- (22) Zhang, B.; Zhang, J.; Zhong, Z.; Zhang, Y.; Song, M.; Wang, X.; Ding, K.; Ruan, R. Conversion of Poultry Litter into Bio-Oil by Microwave-Assisted Catalytic Fast Pyrolysis Using Microwave Absorbent and Hierarchical ZSM-5/MCM-41 Catalyst. *J. Anal. Appl. Pyrolysis* 2018, 130, 249–255.
- (23) Inagaki, S.; Shinoda, S.; Kaneko, Y.; Takechi, K.; Komatsu, R.; Tsuboi, Y.; Yamazaki, H.; Kondo, J. N.; Kubota, Y. Facile Fabrication of ZSM-5 Zeolite Catalyst with High Durability to Coke Formation During Catalytic Cracking of Paraffins. ACS Catal. 2013, 3 (1), 74–78
- (24) Shao, S. S.; Zhang, H. Y.; Heng, L. J.; Luo, M. M.; Xiao, R.; Shen, D. K. Catalytic Conversion of Biomass Derivates over Acid Dealuminated ZSM-5. *Ind. Eng. Chem. Res.* **2014**, *53* (41), 15871–15878.
- (25) Lu, Y.; Fan, H.; Stump, A.; Ward, T. L.; Rieker, T.; Brinker, C. J. Aerosol-Assisted Self-Assembly of Mesostructured Spherical Nanoparticles. *Nature* **1999**, 398 (6724), 223–226.
- (26) Debecker, D. P.; Le Bras, S.; Boissiere, C.; Chaumonnot, A.; Sanchez, C. Aerosol Processing: A Wind of Innovation in the Field of Advanced Heterogeneous Catalysts. *Chem. Soc. Rev.* **2018**, *47* (11), 4112–4155.
- (27) Smeets, V.; Baaziz, W.; Ersen, O.; Gaigneaux, E. M.; Boissiere, C.; Sanchez, C.; Debecker, D. P. Hollow Zeolite Microspheres as a Nest for Enzymes: A New Route to Hybrid Heterogeneous Catalysts. *Chemical Science* **2020**, *11* (4), 954–961.
- (28) Aghamohammadi, S.; Haghighi, M. Spray-Dried Zeotype/Clay Nanocatalyst for Methanol to Light Olefins in Fluidized Bed Reactor: Comparison of Active and Non-Active Filler. *Appl. Clay Sci.* **2019**, 170, 70–85.
- (29) Xiong, G.; Yin, J. P.; Liu, J. X.; Liu, X. Y.; Guo, Z. D.; Liu, L. P. Aerosol-Assisted Synthesis of Nano-Sized ZSM-5 Aggregates. *RSC Adv.* **2016**, *6* (103), 101365–101371.
- (30) Niu, C.; Liu, M.; Gao, X.; Ye, X.; Wen, Y.; Liu, Y.; Wang, X. Fabrication of Microspheres by Nano-TS-1 Crystals Via a Spray-Forming Process: From Screening to Scale-Up. *ACS Omega* **2019**, *4* (2), 4397–4404.
- (31) Hargreaves, J. S. J.; Munnoch, A. L. A Survey of the Influence of Binders in Zeolite Catalysis. *Catal. Sci. Technol.* **2013**, 3 (5), 1165–1171
- (32) Zhang, G.; Li, J.; Zhang, G.; Zhao, L. Room-Temperature Synthesis of Ni Nanoparticles as the Absorbent Used for Sewage Treatment. *Adv. Mater. Sci. Eng.* **2015**, 2015, 1–4.
- (33) Su, Y.; Wang, Y.; Owoseni, O.; Zhang, Y.; Gamliel, D. P.; Valla, J. A.; McPherson, G. L.; John, V. T. A Bottle-around-a-Ship Method to Generate Hollow Thin-Shelled Particles Containing Encapsulated Iron Species with Application to the Environmental Decontamination

- of Chlorinated Compounds. ACS Appl. Mater. Interfaces 2018, 10 (16), 13542-13551.
- (34) Li, X. C.; John, V. T.; He, G. H.; He, J. B.; Spinu, L. Magnetic Tio2-Sio2 Hybrid Hollow Spheres with Tio2 Nanofibers on the Surface and Their Formation Mechanism. *J. Mater. Chem.* **2012**, 22 (34), 17476–17484.
- (35) Farinmade, A.; Ojo, O. F.; Trout, J.; He, J. B.; John, V.; Blake, D. A.; Lvov, Y. M.; Zhang, D. H.; Nguyen, D.; Bose, A. Targeted and Stimulus-Responsive Delivery of Surfactant to the Oil-Water Interface for Applications in Oil Spill Remediation. *ACS Appl. Mater. Interfaces* **2020**, *12* (1), 1840–1849.
- (36) Ojo, O. F.; Farinmade, A.; Trout, J.; Omarova, M.; He, J. B.; John, V.; Blake, D. A.; Lvov, Y. M.; Zhang, D. H.; Nguyen, D.; Bose, A. Stoppers and Skins on Clay Nanotubes Help Stabilize Oil-in-Water Emulsions and Modulate the Release of Encapsulated Surfactants. *ACS Applied Nano Materials* **2019**, 2 (6), 3490–3500.
- (37) Saha, S.; Pal, A.; Kundu, S.; Basu, S.; Pal, T. Photochemical Green Synthesis of Calcium-Alginate-Stabilized Ag and Au Nanoparticles and Their Catalytic Application to 4-Nitrophenol Reduction. *Langmuir* **2010**, *26* (4), 2885–93.
- (38) Du, Y.; Chen, H.; Chen, R.; Xu, N. Synthesis of P-Aminophenol from P-Nitrophenol over Nano-Sized Nickel Catalysts. *Appl. Catal., A* **2004**, 277 (1–2), 259–264.
- (39) Gamliel, D. P.; Bollas, G. M.; Valla, J. A. Bifunctional Ni-ZSM-5 Catalysts for the Pyrolysis and Hydropyrolysis of Biomass. *Energy Technology* **2017**, *5* (1), 172–182.
- (40) Gamliel, D. P.; Wilcox, L.; Valla, J. A. The Effects of Catalyst Properties on the Conversion of Biomass Via Catalytic Fast Hydropyrolysis. *Energy Fuels* **2017**, *31* (1), 679–687.
- (41) Hardenberg, T. A. J.; Mertens, L.; Mesman, P.; Muller, H. C.; Nicolaides, C. P. A Catalytic Method for the Quantitative Evaluation of Crystallinites of ZSM-5 Zeolite Preparations. *Zeolites* **1992**, *12* (6), 685–689.
- (42) Jesudoss, S. K.; Vijaya, J. J.; Kaviyarasu, K.; Kennedy, L. J.; Jothi Ramalingam, R.; Al-Lohedan, H. A. Anti-Cancer Activity of Hierarchical ZSM-5 Zeolites Synthesized from Rice-Based Waste Materials. *RSC Adv.* **2018**, *8* (1), 481–490.
- (43) Tian, Y.; Liu, Y.; Pang, F.; Wang, F.; Zhang, X. Green Synthesis of Nanostructed Ni-Reduced Graphene Oxide Hybrids and Their Application for Catalytic Reduction of 4-Nitrophenol. *Colloids Surf., A* **2015**, *464*, 96–103.
- (44) Ji, X.; Hu, Q.; Hampsey, J. E.; Qiu, X.; Gao, L.; He, J.; Lu, Y. Synthesis and Characterization of Functionalized Mesoporous Silica by Aerosol-Assisted Self-Assembly. *Chem. Mater.* **2006**, *18* (9), 2265–2274
- (45) Bore, M. T.; Marzke, R. F.; Ward, T. L.; Datye, A. K. Aerosol Synthesized Mesoporous Silica Containing High Loading of Alumina and Zirconia. *J. Mater. Chem.* **2005**, *15* (47), 5022–5028.
- (46) Kruk, M.; Jaroniec, M.; Sakamoto, Y.; Terasaki, O.; Ryoo, R.; Ko, C. H. Determination of Pore Size and Pore Wall Structure of MCM-41 by Using Nitrogen Adsorption, Transmission Electron Microscopy, and X-Ray Diffraction. *J. Phys. Chem. B* **2000**, *104* (2), 292–301.
- (47) Gou, J.; Wang, Z.; Li, C.; Qi, X.; Vattipalli, V.; Cheng, Y.-T.; Huber, G.; Conner, W. C.; Dauenhauer, P. J.; Mountziaris, T. J.; Fan, W. The Effects of ZSM-5 Mesoporosity and Morphology on the Catalytic Fast Pyrolysis of Furan. *Green Chem.* **2017**, *19* (15), 3549–3557
- (48) Yu, L.; Farinmade, A.; Ajumobi, O.; Su, Y.; John, V. T.; Valla, J. A. MCM-41/ZSM-5 Composite Particles for the Catalytic Fast Pyrolysis of Biomass. *Appl. Catal., A* **2020**, *602*, 117727.